Grain size dependence of magnetic properties in shock synthesized bulk $Pr_2Fe_{14}B/\alpha$-Fe nanocomposites

Z. Q. Jin
School of Materials Science and Engineering, Georgia Institute of Technology, Atlanta, Georgia 30332 and Department of Physics, University of Texas at Arlington, Arlington, Texas 76019

N. N. Thadhani,[a] M. McGill, J. Li, Y. Ding, and Z. L. Wang
School of Materials Science and Engineering, Georgia Institute of Technology, Atlanta, Georgia 30332

H. Zeng and M. Chen
IBM T. J. Watson Research Center, Yorktown Heights, New York 10598 and Department of Physics, University of Texas at Arlington, Arlington, Texas 76019

S. F. Cheng
Naval Research Laboratory, Washington, District of Columbia 20375

J. P. Liu[b]
Department of Physics, University of Texas at Arlington, Arlington, Texas 76019

(Received 29 March 2004; accepted 18 June 2004)

The structural and magnetic properties of the melt-spun $Pr_2Fe_{14}B/\alpha$-Fe nanocomposite powders consolidated via shock-wave compression and subjected to postshock thermal treatment were investigated. Shock compression results in grain refinement, which leads to a reduction of an effective anisotropy and therefore an increase in the ferromagnetic exchange length, resulting in an enhanced exchange coupling in fully consolidated bulk magnets. A small amount of amorphous phase formed during the shock compression were observed to crystallize into $Pr_2Fe_{14}B$ upon annealing above 600 °C. The heat treatment also results in the recovery of coercivity partially lost during the consolidation, which can be related directly to the dependence of the effective anisotropy on the grain size, as illustrated by the transmission electron microscopy observation of grain refinement in the shock-consolidated bulk samples. A uniform grain morphology is suggested as a means for further increasing the magnetic properties of bulk nanocomposites. © *2004 American Institute of Physics*. [DOI: 10.1063/1.1782956]

I. INTRODUCTION

A favorable combination of high magnetization and large magnetic anisotropy allows intermetallic compounds such as $R_2Fe_{14}B$ (R=Pr,Nd) to be widely used in commercial applications. Exchange-coupled nanocomposites based on R—Fe—B offer the potential for a considerable enhancement of the maximum energy product $(BH)_{max}$ over the $R_2Fe_{14}B$ single-phase magnets because of the enhanced remanence.[1–4] These nanocomposites consisting of the hard magnetic $R_2Fe_{14}B$ grains and the soft magnetic α-Fe phase are usually made in the form of powders, ribbons, and thin films, produced by means of mechanical alloying, melt spinning, and sputtering, respectively.[5–8] The preparation of bulk magnets then requires resin bonding, hot pressing, or other methods of powder consolidation, which nevertheless deteriorate the magnetic properties due to either the dilution of the magnetization caused by additives of nonmagnetic resin or the grain growth caused by prolonged thermal excursions.

The shock-wave compression of powders is a technique that is ideally suited for making the bulk nanocrystalline materials.[9–13] Since the consolidation of powders occurs in the time scale of shock pulse duration of microseconds, the powders are not subjected to long-term thermal excursions; grain growth is thus minimized. Recently, we have investigated the shock compression of exchange-coupled Pr-Fe-B-based nanocomposite powders and obtained bulk magnets with nearly full density,[14] while retaining nanostructured morphology and even achieving slight grain refinement in the shock-consolidated bulk compacts.

It is well known that the grain size of the hard and the soft ferromagnetic components has critical influence on exchange interactions and on magnetic properties, especially on the remanence, effective anisotropy, and coercivity of nanocomposites.[15–18] In order to obtain a higher energy product, a fine grain size is necessary for the nanocomposite magnets. Sun *et al.*[16] investigated experimentally the dependence of coercivity on the grain size of the soft magnetic α-Fe in mechanically alloyed $(Nd,Dy)(Fe,Co,Nb,B)_{5.5}/\alpha$-Fe magnets and pointed out that there exists an optimum grain size around 15 nm with which the best magnetic properties can be obtained. With further reduction in the grain size, the remanence and the maximum energy product increase while the effective anisotropy and the coercivity may decrease. In the event that the coercivity is less than half of the remanence, the energy product drastically deteriorates due to the limitation of the irreversible demagnetization processes.[15] Since shock consolidation results in the retention and even in

[a]Electronic mail: naresh.thadhani@mse.gatech.edu
[b]Electronic mail: pliu@uta.edu

some refinement of the grain size, postshock heat treatments can be employed to adjust the grain size and to optimize the magnetic properties. The motivation of the present work is to gain insight into the possible changes in microstructure during the postshock heat treatment of the shock-compressed compacts. In this work, the grain size dependence of the coercivity in the shock-consolidated bulk magnets was investigated so as to verify the effect of the grain refinement on the magnetic properties of the shock-compacted nanocomposite samples.

II. EXPERIMENTAL PROCEDURE

$Pr_2Fe_{14}B$-based nanocomposite ribbons with an excess of 20 wt % α-Fe were fabricated by melt spinning. The melt-spun ribbons were pulverized into powders and cold pressed into a three-capsule fixture for the shock consolidation using the Georgia Tech 80-mm-barrel-diameter single-stage gas gun, equipped with a catch tank for soft recovery of the consolidated samples. The shock consolidation experiments were performed at an impact velocity of 880 m/s (average calculated peak pressure of ~20 GPa), resulting in nearly full dense compacts. Sections cut from the recovered bulk specimens were subjected to subsequent thermal treatment at temperatures from 400 to 700 °C for different times. Prior to annealing, the sectioned samples were sealed into the evacuated quartz tubes and were placed in a furnace preheated to desired temperatures. After being held for the desired time and temperature, the quartz tubes were taken out and cooled in air. In order to observe evidence of any structural changes caused by the heat treatment, the differential thermal analysis (DTA) was performed using the Perkin-Elmer DTA7 at a heating rate of 20 K/min. The annealed samples were characterized by x-ray diffraction (XRD) using CuKα radiation, scanning electron microscopy (SEM), and transmission electron microscopy (TEM). X-ray diffraction line broadening analysis, using the Williamson-Hall method,[19] was also performed to determine the retained microstrain, and to estimate the crystallite size. The magnetic properties were measured using a superconducting quantum interference device (SQUID) magnetometer with a field of up to 70 kOe. The magnetic properties measurement data was adjusted by using the effective demagnetization factors of 0.33 and 0.14 for starting powders and for shock-compacted samples, respectively, determined experimentally and estimated according to the sample morphology.

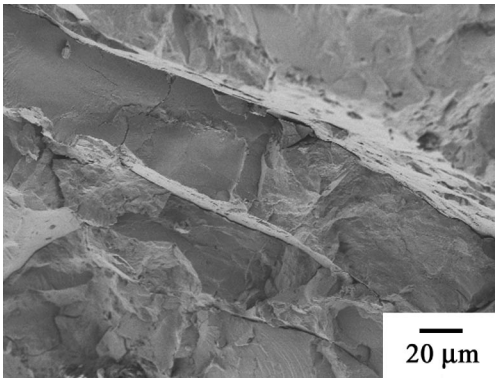

FIG. 1. Typical SEM image of a shock-compacted sample following annealing at 700 °C for 20 min.

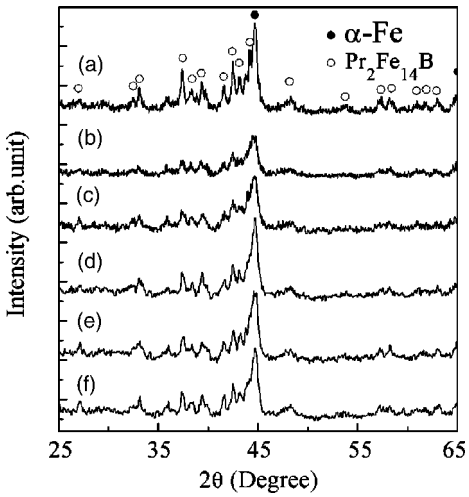

FIG. 2. XRD patterns of the starting material (a), the as-compacted (b), and the postshock annealed samples with thermal treatment for 1 h at 400 °C (c), and for 20 min at 600 °C (d), 650 °C (e), and 700 °C (f).

III. RESULTS AND DISCUSSIONS

Figure 1 shows the SEM micrograph of the fracture surface of the annealed shock-consolidated compacts. The layered morphology and solid-state bonding between flakes are observed in the samples, resulting in relative densities of up to 98%–99% of the theoretical mass density. The layered morphology formed during the initial uniaxial packing process is retained during the subsequent shock loading and thermal treatment.

XRD patterns of the starting material and the shock-compressed and annealed samples are shown in Fig. 2. All of the samples consist of magnetic $Pr_2Fe_{14}B$ (2:14:1) and α-Fe phases. The broadened peaks are the characteristics of the as-compacted samples, indicating a structure of very fine crystallites and possibly a small amount of amorphous phase. The existence of the amorphous phase formed during the shock consolidation was checked by the DTA. The DTA of the sample before the shock compression as shown in Fig. 3

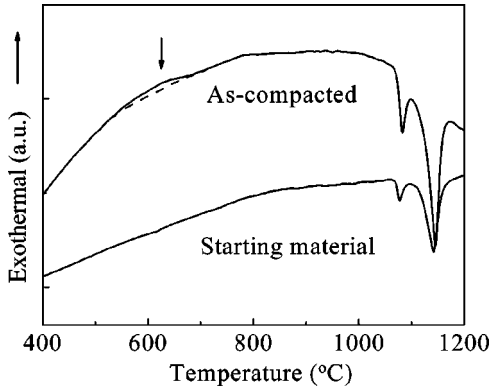

FIG. 3. DTA traces on the starting material and on the shock-compacted sample, illustrating the crystallization of amorphous phase in the latter sample.

reveals only two endothermal peaks at high temperatures, which may be related to the melting of the 2:14:1 phase at 1080 °C and of the iron at 1140 °C, respectively. These peaks are also observed in the shock-compressed samples, showing not much difference in the components of the primary phases upon the shock compression. However, a small exothermic bump seems to be visible around 620 °C (as marked by the arrow) in the shock-compacted sample. The wide signal of an exothermic bump has been observed for several shock-compacted samples while it is too weak for further investigation on the phase transformation. The exothermic effect may arise from the crystallization of the amorphous phase formed during the shock compaction process and actually is close to the crystallization temperature of 2:14:1 crystallites from the amorphous phase.[20] Apparently, the amount of amorphous phase formed during the high-strain-rate shock loading is not enormous because the shock energy dissipates not only in the form of configurational changes in the particles but also in the forms of interparticle friction and bonding accompanied by the annihilation of voids via plastic flow and the dispersion of fragments. Moreover, during the subsequent heating process, pre-existed nanocrystallites in the shock-compacted samples serve as the nucleation centers and result in the high concentration gradient at grain boundary of the nanocomposites. Wang *et al.*[21] pointed out that a sharp concentration gradient of Nd atoms may reduce or even eliminate the thermodynamic driving force for crystallite nucleation. These may explain that the crystallization trace on the DTA curve in this study is not as evident as those that occurred for fully amorphous samples.[20]

After postshock thermal treatments, the phase component is observed to remain almost the same as shown in Fig. 2, except the variation in peak intensity that illustrates a different fraction of the hard/soft magnetic phases in the nanocomposite. Peak broadening is still visible for the sample annealed at 400 °C for 1h, but it narrows upon annealing above 600 °C. Meanwhile, an increased intensity in the α-Fe reflections is observed, which can be attributed to an increase in the amount of α-Fe crystallites. At temperature above 650 °C, the peak intensity ratio of $2:14:1/\alpha$-Fe phases increases slightly, showing the formation of more 2:14:1 crystallites. The average grain size ($\sim$25 nm) calculated by the XRD line broadening analysis for the samples annealed at 700 °C is slightly larger than those of the as-compacted samples ($\sim$20 nm) due to the dissolution of the small grains by the large grains.

Pressure gradients produced during the shock consolidation of powders can lead to the generation of the large residual stresses. This effect has also been revealed in our previous work[14] as well as that of others.[22] The retained plastic strain in the pre- and postshock compacts can be estimated by the slope of the Williamson-Hall plots shown in Fig. 4. The error bars in the figure indicate the scatter in the measured data of the XRD peak width. The shock compaction induces a large amount of strain in the bulk materials. After the annealing treatment, the strain relaxation is observed as revealed by the decrease in the slope of the $B\cos\theta - \sin\theta$ plot.

Our previous TEM observation reveals the grain refinement and the irregular grain morphology in the samples subjected to the shock compaction.[14] Figures 5(a) and 5(b) show the TEM micrographs of the shock-compacted samples annealed at 700 and 800 °C, respectively. The diffraction pattern shows isotropic characteristic. The subsequent heat treatment does not change the grain morphology while the grain size coarsens with the increasing annealing temperature. The quantitative analysis of the microstructure of the samples revealed the different grain size distribution for these samples. The distributions of the grain size before and after the heat treatment in comparison with the starting materials are shown in Fig. 6. The starting materials show a Gaussian distribution with the maximum at grain size of 23 nm. However, the grains for the as-compacted samples illustrate a bimodal distribution centered at two characteristic maxima (8 and 18 nm). The grain size refinement is attributed to the fragmentation and shearing of nanocrystallites

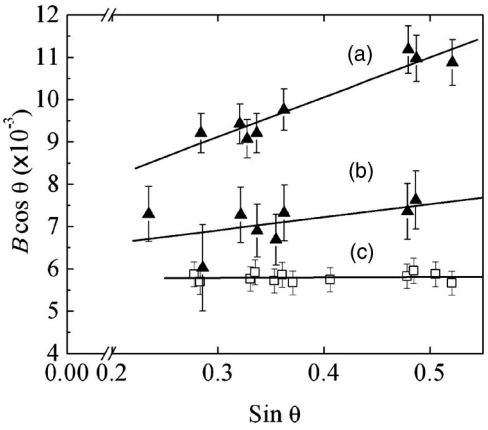

FIG. 4. Williamson-Hall plots of the shock-compacted sample (a) and the compact annealed at 700 °C for 20 min (b) compared with the starting materials (c).

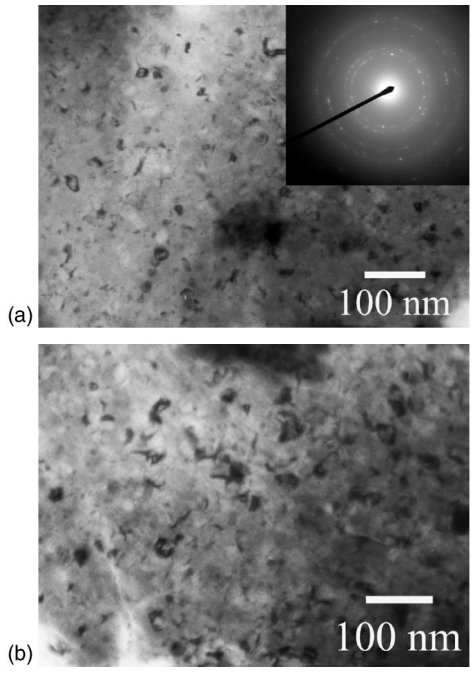

FIG. 5. TEM micrographs of the shock-compacted samples annealed at 700 °C (a) and 800 °C (b).

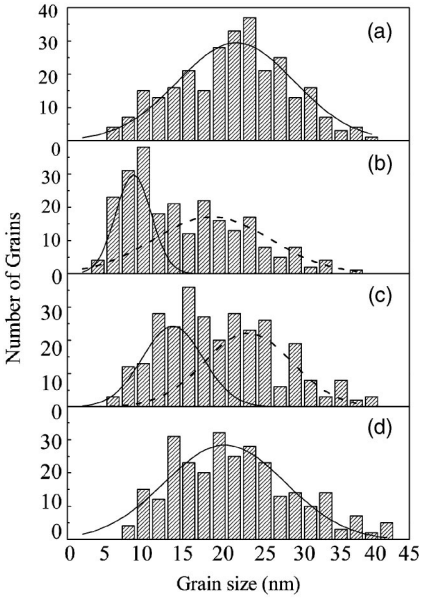

FIG. 6. Histogram comparing the grain size distributions of the starting materials (a), the as-compacted samples (b), and the compacts annealed at 700 °C (c) and 800 °C (d).

during the dynamic compaction.[14] The high resolution TEM (HRTEM) image (Fig. 7) of the as-compacted sample illustrates that the small grains correspond to α-Fe, whereas the others correspond to $Pr_2Fe_{14}B$ phase. This is also consistent with the volume fractions of $Pr_2Fe_{14}B$ and α-Fe (20 wt %) in the nanocomposite compacts. Although the amorphous phase (AM) is observed in the compacted nanocomposite samples, it is difficult to precisely estimate the amount of amorphous phase directly from the HRTEM observation. However, it can be assumed from the XRD patterns that the amorphous phase is less in the annealed samples due to the crystallization. After annealing at 700 °C, a slight increase in the grain size for both the hard and the soft phases is observed; the diameter of the small particles increased from about 8 nm to 14 nm, and that of the larger particles increased from about 18 nm to 23 nm after annealing. For heat treatment at 800 °C, the bimodal feature of the histogram is less pronounced, and more likely, a Gaussian distribution is observed while a greater fraction of the larger grains

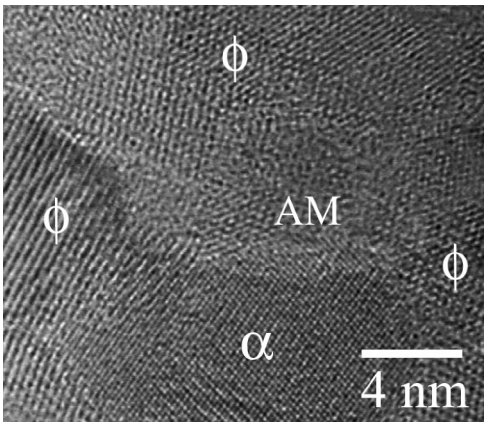

FIG. 7. HRTEM image of the as-compacted samples showing the existence of the α-Fe (α), 2:14:1 phase (ϕ) and amorphous phase (AM).

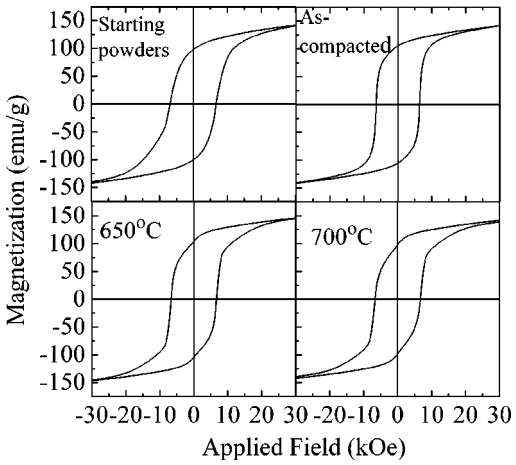

FIG. 8. Hysteresis loops of the starting powders, the shock-compacted samples, and the compacts annealed at 650 and 700 °C for 20 min, respectively.

(>25 nm) exists due to the high annealing temperature. This observation shows that the grain size of both $Pr_2Fe_{14}B$ and α-Fe increases slightly with the annealing temperature, although it is still not significantly larger than that of the starting materials.

The typical hysteresis loops of the starting material, the as-compacted, and the annealed samples are shown in Fig. 8. It can be seen that the as-compacted sample shows smooth loops, indicating an effective exchange coupling, whereas the demagnetization curves of the annealed samples show a small kink at zero field, indicating a partial decoupling due to the presence of some larger grains. The highest remanence is observed in the as-compacted samples, which results in the enhanced exchange coupling between the $Pr_2Fe_{14}B$ and the α-Fe grains and the highest energy product of 16.3 MGOe. It is well known that for an optimum exchange coupling, the size of the soft magnetic α-Fe grains should be approximately the order of the effective exchange range $L_{ex} \approx \pi(A_{\text{eff}}/K_{\text{eff}})^{1/2}$, where A_{eff} denotes the effective exchange stiffness and K_{eff} is the effective anisotropy constant that originates from the contribution of the hard and the soft magnetic components of the nanocomposite magnets.[16,23] Gao *et al.*[17] analyzed the dependence of the effective anisotropy on the grain size of nanocomposites and concluded that K_{eff} decreases with the reduction in the grain size D. Under this circumstance, the effective exchange range L_{ex} increases, thus more grains can be exchange coupled, leading to the increase of the remanence and the maximum energy product. As expected, the improved magnetic properties are observed in the as-compacted sample with finer grain size. However, when the grain size D of the α-Fe is smaller than the effective exchange range L_{ex}, an overlap of exchange field between two hard magnetic grains situated at the opposite sides of the soft grains occurs.[16] This results in a decrease of the coercivity in the as-compacted samples (6.4 kOe) as compared with that (6.8 kOe) of the starting materials as shown in Fig. 9. This is very similar to the results reported by Sun *et al.* for the nanocomposite $Nd_2Fe_{14}B/\alpha$-Fe magnets.[16]

Figure 9 plots the overall magnetic properties of the starting material, the as-compacted, and the annealed

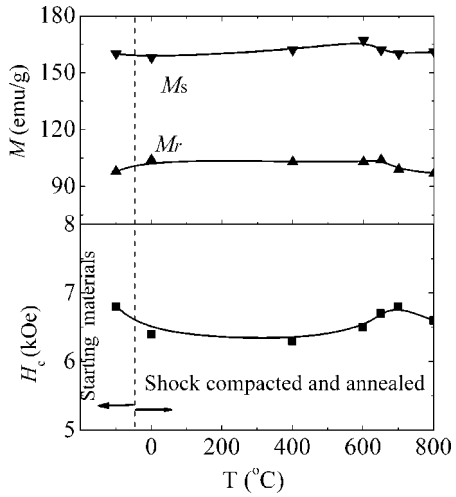

FIG. 9. Annealing temperature dependence of the magnetic properties for the shock-compacted samples.

samples. Saturation magnetization M_s increases slightly with the annealing temperature up to 600 °C due to the precipitation of α-Fe from amorphous phase and then decreases due to the formation of more $Pr_2Fe_{14}B$ crystallites above the crystallization temperature. Further increase of the annealing temperature only results in the grain growth and in the deterioration of the remanence. However, it appears that the coercivity of the annealed samples increases with the increasing annealing temperature above 600 °C in the studied range, and it reaches the highest value of 6.8 kOe at 700 °C, which is almost the same as that of the starting materials.

The mechanism controlling coercivity is mainly determined by the fraction of the hard magnetic phase and the grain size of the soft phase and the grain morphology. With consideration of amorphous phase as the soft phase, the actual total fraction of the hard magnetic 2:14:1 phase does not change much when the samples are annealed below the crystallization temperature of 620 °C (Fig. 3). A sterner consideration is for samples annealed above 650 °C, at which the fraction of the hard phases remains the same since no new phase transformation takes place. Moreover, the heat treatment does not significantly alter the grain morphology, except for the grain growth. Therefore, the change in the coercivity after treatment above 650 °C is most likely attributed to the change of the grain size. This can be interpreted in accordance with[24]

$$H_c = 2\alpha_k \alpha_{\text{eff}} K_1/\mu_0 M_s - N_{\text{eff}} M_s,$$

where K_1 and M_s are the anisotropy and the saturation magnetization of the material, α_k, α_{eff}, and N_{eff} are the microstructure-dependent parameters, representing the effect of the anisotropy, the exchange coupling, and the local internal stray field, respectively. For the magnetic nanocomposites, K_1 can be considered as the effective anisotropy K_{eff} as a constant averaged over the various components of nanocomposites. For nanocomposites with volume fractions of the hard and the soft phases being f_h and f_s, the K_{eff} can be simply written as $K_{\text{eff}} = f_h K_{1(Pr_2Fe_{14}B)} + f_s K_{1(Fe)}$. The theoretical calculation on the $Nd_2Fe_{14}B/\alpha$-Fe nanocomposite has shown that all the anisotropic constants, K_{eff}, $K_{1(Nd_2Fe_{14}B)}$, and $K_{1(Fe)}$, increase monotonously, even by above twice the original values when the grain size increases from 10 to 25 nm.[17] Assuming similar conditions for the PrFeB- and NdFeB-based nanocomposites, it is reasonable that the effective anisotropic constant K_{eff} in our case has the same grain size dependence. Apparently, the average grain size of the sample annealed above 600 °C is larger than that of the as-compacted samples, and this leads to the higher coercivity. This is in good agreement with the previous observation on the mechanically milled $Nd_2Fe_{14}B/\alpha$-Fe nanocomposites. Sun *et al.*[16] reported that for the ultrafine grain size D of the α-Fe (below $2L_{ex} \sim 15$ nm), the coercivity is very low due to the coupling between hard magnetic grains situated at two sides of a soft grain and the coercivity increases with the grain growth up to 25 nm for the volume fraction of the α-Fe in the range of 30%–70%. It is reasonable that the grain growth also results in the modification of the local environments of the grain boundaries and the change of the microstructure-related parameters α_k, α_{eff}, and N_{eff}. So the variation in the characteristic of the coercivity along with the grain size may not have a linear relation with the anisotropy constant. It means that the coercivity does not increase significantly while the effective anisotropy constant is doubled when the grain size increases from 10 to 25 nm. A uniform grain morphology with larger α_k and with smaller N_{eff} is suggested as a means for further increasing the coercivity of bulk nanocomposites. A decrease of the coercivity above 800 °C was observed due to the excessive grain growth and to the existence of the free zones within the soft phase grains. The free zone acts as the reversal nucleation center, and the magnetization reversal nucleates at relatively lower fields over the soft phase, resulting in the reduction of the coercivity. This observation suggests that the optimal coercivity may be obtained with a narrow grain size distribution of 10–25 nm. The consequence of the excessive grain growth is the occurrence of kinked hysteresis loops as shown in Fig. 9. Therefore, low annealing temperature around crystallization temperature is necessary for retaining optimal combination of the coercivity and the maximum energy product.

In order to achieve higher energy product in the shock-compacted isotropic nanocomposite magnets, two approaches may be considered. One is to enhance the remanence by further grain refinement and meanwhile to achieve a narrow grain size distribution. However, the variation of the remanence with respect to the changes of the grain size conflicts with the grain size dependence of the effective anisotropy and coercivity. This means that it is difficult to optimize the magnetic properties solely by grain size reduction. Another feasible way is to increase the coercivity by reducing the local stray fields at the edges and corners of the irregular grains, i.e., a uniform grain morphology is needed, since a regular grain microstructure generally leads to a higher α_k, α_{eff}, and lower N_{eff}, thus a larger coercivity may be expected whereas the remanence is not influenced remarkably by the type of grain structure.

IV. CONCLUSION

The effects of thermal treatment on the structure and on the magnetic properties of the shock-compacted

$Pr_2Fe_{14}B/\alpha$-Fe nanocomposite powders have been investigated in this work. Subsequent annealing results in strain relaxation. The shock compaction leads to the enhancement of exchange coupling due to the grain refinement and higher energy product at the expense of anisotropy and coercivity. The coercivity increases after heat treatment due to the grain growth induced enhancement of the anisotropy. In order to achieve higher magnetic properties, a uniform grain morphology and a narrow grain size distribution are suggested.

ACKNOWLEDGMENT

This work is supported by the US DoD/DARPA through Army Research Office (ARO) under Grant No. DAAD19-03-1-0038.

[1]R. Skomski and J. M. D. Coey, Phys. Rev. B **48**, 15812 (1993).
[2]E. F. Kneller and R. Hawig, IEEE Trans. Magn. **27**, 3588 (1991).
[3]T. Schrefl, H. Kronmüller, and J. Fidler, J. Magn. Magn. Mater. **127**, L273 (1993).
[4]I. Panagiotopoulos, L. Withanawasam, and G. C. Hadjipanayis, J. Magn. Magn. Mater. **152**, 353 (1996).
[5]Z. Q. Jin, H. Okumura, H. L. Wang, and G. C. Hadjipanayis, J. Appl. Phys. **91**, 8165 (2002).
[6]P. G. McCormick, W. F. Miao, P. A. I. Smith, J. Ding, and R. Street, J. Appl. Phys. **83**, 6256 (1998).
[7]J. P. Liu, C. P. Luo, Y. Liu, and D. J. Sellmyer, Appl. Phys. Lett. **72**, 483 (1998).
[8]H. Zeng, J. Li, J. P. Liu, Z. L. Wang, and S. H. Sun, Nature (London) **420**, 395 (2002).
[9]N. N. Thadhani, J. Appl. Phys. **76**, 2129 (1994).
[10]M. Leonowicz, W. Kaszuwara, E. Jezierska, D. Januszewski, G. Mendoza, H. A. Davies, and J. Paszula, J. Appl. Phys. **83**, 6634 (1998).
[11]N. N. Thadhani, R. A. Graham, T. Royal, E. Dunbar, M. U. Anderson, and T. T. Holman, J. Appl. Phys. **82**, 1113 (1997).
[12]N. N. Thadhani, Mater. Sci. Forum **426–432**, 2357 (2003).
[13]S. I. Shkuratov, E. F. Talantsev, J. C. Dickens, M. Kristiansen, and J. Baird, Appl. Phys. Lett. **82**, 1248 (2003).
[14]Z. Q. Jin, K. H. Chen, J. Li, H. Zeng, S. -F. Cheng, J. P. Liu, Z. L. Wang, and N. N. Thadhani, Acta Mater. **52**, 2147 (2004).
[15]D. Goll, M. Seeger, and H. Kronmüller, J. Magn. Magn. Mater. **185**, 49 (1998).
[16]X. K. Sun, J. Zhang, Y. L. Chu, W. Liu, B. Z. Cui, and Z. D. Zhang, Appl. Phys. Lett. **74**, 1740 (1999).
[17]R. W. Gao *et al.*, J. Appl. Phys. **94**, 664 (2003).
[18]Z. Q. Jin, B. Z. Cui, J. P. Liu, Y. Ding, Z. L. Wang, and N. N. Thadhani, Appl. Phys. Lett. **84**, 4382 (2004).
[19]G. K. Williamson and W. H. Hall, Acta Metall. **1**, 22 (1953).
[20]Z. Q. Jin, H. Okumura, J. S. Muñoz, Y. Zhang, H. L. Wang, and G. C. Hadjipanayis, J. Phys. D **35**, 2893 (2002).
[21]Z. C. Wang, S. Z. Zhou, Y. Qiao, M. C. Zhang, and R. Wang, J. Magn. Magn. Mater. **218**, 72 (2000).
[22]M. A. Meyers, D. J. Benson, and E. A. Olevsky, Acta Mater. **47**, 2089 (1999).
[23]H. Kronmüller, R. Fischer, M. Seeger, and A. Zern, J. Phys. D **29**, 2274 (1996).
[24]J. Bauer, M. Seeger, A. Zern, and H. Kronmüller, J. Appl. Phys. **80**, 1667 (1996).